



RESEARCH ARTICLE

WILEY

Climate impacts on soil erosion and muddy flooding at 1.5 versus 2°C warming

Donal Mullan¹ | Tom Matthews² | Karel Vandaele³ | Iestyn D. Barr⁴ | Graeme T. Swindles⁵ | John Meneely¹ | John Boardman^{6,7} | Conor Murphy⁸

¹School of Natural and Built Environment, Queen's University Belfast, Belfast BT7 1NN, Northern Ireland, UK

²Department of Geography, Loughborough University, Loughborough LE11 3TU, UK

³Watering van Sint-Truiden, 3800 Sint-Truiden, Belgium

⁴School of Science and the Environment, Manchester Metropolitan University, Manchester M15 6BH, UK

⁵School of Geography, University of Leeds, Leeds LS2 9JT, UK

⁶Environmental Change Institute, Oxford University Centre for the Environment, University of Oxford, Oxford OX1 3QY, UK

⁷Department of Geography, University of the Free State, PO Box 339, Bloemfontein 9300, South Africa

⁸Department of Geography, Maynooth University, Maynooth, Ireland

Correspondence

Donal Mullan, School of Natural and Built Environment, Queen's University Belfast, Belfast, BT7 1NN, Northern Ireland, UK. Email: d.mullan@qub.ac.uk

Funding information

British Society for Geomorphology

Abstract

Following the 2015 'Paris Agreement' that seeks to contain global mean temperature increase (GMTI) to well below 2°C and more ambitiously within 1.5°C, recent studies have begun assessing the response of various sectors to these levels of warming. Most studies have so far concentrated on temperature-sensitive sectors. Given the links between a warmer atmosphere and rainfall intensity, there is also a need to examine impact sectors driven primarily by changing rainfall characteristics. One example is soil erosion and muddy flooding from agricultural land, which damages the natural and built environment. Using a case-study hillslope in eastern Belgium—an area particularly impacted by muddy floods—this study examines (a) whether soil erosion and muddy flooding will increase in the future; and (b) whether containing GMTI to 1.5°C would help limit the problem versus 2°C. The Water Erosion Prediction Project model was used to simulate muddy flooding for the present-day and under a range of future scenarios derived from climate models that correspond to 1.5 and 2°C GMTI. The main findings reveal no statistically significant differences between muddy flooding at 1.5 and 2°C GMTI. Limiting GMTI to 1.5°C therefore does not appear to make much difference to soil erosion and muddy flooding, because the timing of changing rainfall intensity does not always follow clear patterns with increased warming. Regardless of the magnitude of future warming, an earlier and longer muddy flooding season is projected—highlighting that mitigation measures should be continually adapted to remain resilient to climate change.

KEYWORDS

climate change, muddy flooding, rainfall, sediment yield, soil erosion

1 | INTRODUCTION

Robust appraisals of climate impacts at varying levels of global mean temperature increase (GMTI) are important in assessing the resilience of many sectors to climate change and in planning appropriate adaptation strategies. At the 21st Conference of Parties of the UN Framework Convention on Climate Change (UNFCCC), 195 countries pledged to contain GMTI to 'well below' 2°C above preindustrial levels, and to pursue efforts to further limit warming to 1.5°C (UNFCCC, 2015). Studies examining the impacts of 2°C warming

have increased in recent years, as well as comparative studies with higher levels of warming including 4°C and above (e.g., James et al., 2015; New, Liverman, Schroeder, & Anderson, 2011). There has been far less attention to impacts from a GMTI of 1.5°C. This is unsurprising given that even the lowest of the representative concentration pathways (RCPs)—used as the drivers for climate projections in the Intergovernmental Panel on Climate Change (IPCC) Fifth Assessment Report (AR5; IPCC, 2013)—projects GMTI above 1.5°C. Investigating the impacts from 1.5°C warming has now become a pressing research area, with the IPCC preparing a special report due for

publication in 2018 “on the impacts of global warming of 1.5°C above preindustrial levels and related greenhouse gas emission pathways.”

1.1 | Soil erosion and muddy flooding

Although there is a clear need to study temperature-sensitive sectors such as agriculture and energy, it is also important to examine sectors driven primarily by changing rainfall characteristics. Extreme rainfall in particular is highly connected to temperature because the saturated vapour pressure of the atmosphere increases at a rate of approximately 7% per 1°C, or more formally 7% K—the so-called Clausius–Clapeyron (CC) relation. This does not translate simply into the same rate for rainfall intensity, which normally shows a sub-CC rate of change, for example, Sun, Solomon, Dai, and Portmann (2007). However, Lenderink and van Meijgaard (2008) found a ‘super-CC’ rate of up to 14% K for the most extreme precipitation events. It could therefore be expected that processes driven by intense precipitation events will increase in magnitude in a warmer climate. Among the processes where rainfall intensity plays an important role is soil erosion from agricultural land. Soil erosion is a major environmental threat to the sustainability and productive capacity of agriculture, with global estimates of around 10 million hectares of cropland being lost to erosion annually (Pimentel, 2006; Yang, Kanae, Oki, Koike, & Musiak, 2003) at a rate ~20 times that of soil formation (Govers, Merckx, van Wesemael, & van Oost, 2017). Although these ‘on-site’ impacts of soil erosion tend to be most prevalent in the (sub) tropics, more temperate regions experience greater problems from the ‘off-site’ impacts (Mullan, Favis-Mortlock, & Fealy, 2012). These impacts relate to the damage caused by soil leaving the field, including sediment and associated nutrients discharging into nearby streams and rivers. This reduces water quality through (a) the build-up of fine sediment in gravel-bedded rivers, reducing breeding sites for salmonid species; and (b) the runoff of nitrates and transport of sediments with adsorbed phosphates into water bodies promoting algal bloom and eutrophication. The off-site impacts of soil erosion also affect people in a more direct way through ‘muddy flooding’ (Boardman, 2010). The term muddy flooding does not have any precise definition, but is generally used to describe the mix of runoff and sediment generated on bare or partially vegetated agricultural fields following heavy and/or prolonged rainfall that results in downslope damage to property, roads, and watercourses (Boardman, 2010). This is particularly problematic in the loess belt of western and central Europe (Boardman, 2010; Boardman, Ligneau, De Roo, & Vandaele, 1994; Boardman, Verstraeten, & Biolders, 2006; Evrard et al., 2010) where silty soils are easily detached and arable crops are sown during times of most intense rainfall. The economic costs of muddy flooding can be considerable, with estimates in central Belgium of up to 16.5 M€ yr⁻¹ in damages to private householders and up to 122 M€ yr⁻¹ to public infrastructure (Evrard, Persoons, Vandaele, & van Wesemael, 2007). Several studies have shown that soil erosion and muddy flooding problems could increase under a changing climate (see Mullan, Favis-Mortlock, and Fealy (2012) and Li and Fang (2016) for examples). These studies typically employ a soil erosion model in

conjunction with future climate scenarios derived from climate models. Given the need for studies examining the varying impacts from 1.5 versus 2°C warming, this study has two aims: (a) to examine whether a statistically significant difference exists between present-day and future rates of muddy flooding; and (b) to examine whether a statistically significant difference exists between soil erosion and muddy flooding at a GMTI of 1.5 versus 2°C. The chosen study site is in the Belgian loess belt—chosen because it is a region where muddy flooding occurs regularly and incurs considerable expense (see above).

2 | METHODS

2.1 | Study area

The Belgian loess belt is a ~9,000 km² plateau with a relatively low mean altitude of 115 m (Figure 1). Based on instrumental climate data for the reference period 1981 to 2010 from Uccle, near Brussels, minimum temperatures are 7°C and maximum temperatures are 15°C (as an annual average), whereas precipitation is 769 mm (with a standard deviation of 169 mm). Rainfall is relatively constant throughout the year, though there is a slight peak in rainfall erosivity from late spring through to early autumn (Verstraeten et al., 2006). Soils are largely loess-derived Haplic Luvisols comprising ~80% silt (World Reference Base, 2014). Arable crops dominate the land cover, with ~65% coverage (Statistics Belgium, 2006). The main crops are spring-sown cereals, industrial and fodder crops including sugar beet, maize, oil-seed rape, chicory, and potatoes (Evrard, Persoons, et al., 2007). Farmers are encouraged to sow cover crops such as phacelia and mustard during the dormant late spring and early summer months to protect the soil whereas summer crops establish (Biolders, Ramelot, & Persoons, 2003).

The site selected for modelling is the Kluiskepel hillslope, located in the 200 km² Melsterbeek catchment in Belgium's Limburg province. It is important to point out that cultivated hillslopes are just one of the two major contributing areas to muddy flooding in the Belgian loess belt—the other being dry zero-order valleys where runoff and sediment transport are concentrated in the thalweg (Evrard, Biolders, Vandaele, & van Wesemael, 2007). In this study, we have focused only on the first kind—muddy flooding from cultivated hillslopes. This is because (a) measured event-based data are available for the selected hillslope to help validate the model, but is lacking for wider catchment areas; and (b) the time and computational efforts involved in parameterising models for catchments is higher than could be afforded under the remit of this case study. The area has been impacted by several muddy floods in recent decades, leading to the implementation of a number of mitigation measures to reduce the problem (Evrard, Biolders, et al., 2007). As determined from a 10 m digital elevation model (DEM) of the site, the slope is 340 m long and 310 m wide, with elevation ranging from 80 to 95 m.a.s.l. and an average steepness of 4.2%. The soil type within the Kluiskepel hillslope is typical of the European Loess Belt, with 81.5% silt and 4.5% organic matter (as determined from lab testing in this study). The long-term mean annual temperature at the nearby station of



FIGURE 1 The study area [Colour figure can be viewed at wileyonlinelibrary.com]

Maastricht is 10°C, with a mean annual precipitation of 769 mm. As determined by interviews with the farmer, a typical crop rotation at the Kluiskepel involves maize followed by soybeans, with a cover crop of grass. A grass buffer strip occupies the lowest lying 21 m of the slope—designed to trap sediment and encourage infiltration of runoff. Ploughing and planting occurs in mid-spring, with crops harvested in mid-autumn.

2.2 | Present-day soil erosion modelling

The WEPP model (Flanagan & Nearing, 1995; v.2008.907) was selected to simulate runoff, soil loss, deposition, and sediment yield (all diagnostics of muddy flooding) for both observed and future climatic conditions. Sediment yield is particularly important because this is the soil that leaves the hillslope and enters the surrounding natural

and built environment. The WEPP is a physically-based, continuous simulation model that simulates hydrology, water balance, plant growth, soil and, erosion at field, hillslope and watershed scales. WEPP was selected because it is the most commonly used model for climate change-soil erosion studies (see introduction) and is used here to simulate 'present-day' and future rates of soil erosion and muddy flooding at Kluiskepel hillslope. WEPP requires four input parameter files representing slope, soil, land management, and climate.

2.2.1 | Slope

A slope profile for Kluiskepel hillslope was developed by extracting length and elevation data from a 10 m resolution DEM based on airborne laser scanning for the area. A higher resolution DEM would have been ideal, but Zhang, Chang, and Wu (2008) showed that a 10 m Light detection and ranging (LiDAR)-derived DEM generated realistic field boundaries, stream networks and hillslopes, and closely matched observed runoff and erosion rates across two small forested catchments in the USA.

2.2.2 | Soil

A soil auger was used to extract 15 cm bulk soil samples to a total depth of 75 cm (i.e., five samples deep). This sampling was undertaken at 18 locations, evenly distributed between the top and bottom of the slope, making a total of 90 soil samples. Lab analysis was then conducted on soil texture and organic matter (OM). Effective hydraulic conductivity, critical shear, and erodibility values were calculated using equations from the WEPP user manual (Flanagan & Livingston, 1995). The soil properties are shown in Table 1.

2.2.3 | Land management

Plant growth parameters for the necessary crops were taken directly from the WEPP plant database (Flanagan & Nearing, 1995). The selected crops were maize 1 year and soybeans the next—the crops grown in the selected field area. Dates for management operations were obtained directly from the farmer. The management file was split into two sections along two different of the same hillslope. The management file for the upper majority of the slope was parameterised based on the crops outlined above, whereas the bottom 21 m of the slope was parameterised as a strip of permanent grass, with values

taken from the WEPP database to represent this land cover. This section of land management represents the 21 m grass buffer strip planted at the base of the Kluiskepel hillslope to act as a mitigation measure for muddy floods from the slope. The key details of the management files in WEPP are shown in Table 2. Crop rotations and dates of farming operations were left unchanged for future WEPP simulations. The reasons for omitting these important indirect effects of climate change are given in Section 4.5.

2.2.4 | Climate

Climate data in WEPP are simulated using the weather generator climate generator (CLIGEN; Nicks, Lane, & Gander, 1995). The CLIGEN produces long sequences of daily synthetic weather series based on the statistical properties of the observed climate. CLIGEN requires a series of input parameters as shown in Table 3. The most important climatic input variables are those relating to precipitation. The CLIGEN requires monthly means, standard deviations, and skewness values for mean precipitation per wet day. Also required to calculate sequences of wet and dry days are the transitional probabilities of a wet day following a wet day ($P_{w/w}$) and a wet day following a dry day ($P_{w/d}$). Finally, monthly maximum half hour precipitation values (MX.5P) and time to peak rainfall intensity values (Time Pk) are required to calculate rainfall intensity. These values are all calculated on a monthly basis with the exception of the 12 Time Pk values. Instead, the Time Pk values describe an empirical probability distribution of the time to peak rainfall intensity as a fraction of storm duration (Yu, 2003). The full list of the CLIGEN input parameters is shown in Table 3.

Climate data were obtained from the Royal Netherlands Meteorological Institute (KNMI) Climate Explorer site, which archives a range of freely available climate datasets. Daily series of maximum and minimum temperatures and precipitation from 1950 to 2016 were taken from the E-OBS high-resolution (0.25°) gridded dataset of daily climate over Europe (Haylock et al., 2008) using coordinates for the grid overlying the field location (as shown in Figure 1). Subhourly precipitation data from 2004 to 2014 were taken from Niel-bij-Sint-Truiden (13 km from Kluiskepel hillslope) to calculate MX.5P and Time Pk. All other variables—wind speed and direction, relative humidity (1906–2014), and solar radiation (1965–2014) were taken from Maastricht in the Netherlands. Maastricht is just 29 km from Kluiskepel hillslope and with no major changes in topography or distance from the coast, it could be expected that both areas have very similar climates. The

TABLE 1 Measured and estimated* input parameters representing soil conditions at Kluiskepel hillslope

Depth (cm)	Clay %	Silt %	Sand %	OM %	Kr (s/m)*	Ki (kg s/m ⁴)*	Tc (n/m ²)*	Kb (mm h ⁻¹)*	Albedo*
0–15	11.2	80.5	8.3	4.5	0.021	5,434,397	3.5	1.62	0.10
16–30	10.9	79.9	9.1	4.2	0.022	5,450,501	3.5	1.70	0.11
31–45	10.5	80.8	8.7	4.2	0.023	5,475,242	3.5	1.66	0.11
46–60	10.5	81.2	8.3	4.8	0.023	5,477,699	3.5	1.63	0.09
61–75	10.2	80.9	8.8	4.8	0.024	5,489,447	3.5	1.67	0.09
Mean	10.7	80.7	8.6	4.5	0.023	5,465,457	3.5	1.66	0.10

Note. Kr = rill erodibility; Ki = interrill erodibility; Tc = baseline critical flow hydraulic shear; Kb = baseline effective hydraulic conductivity

TABLE 2 Management details for Kluiskapel hillslope

Year	Operation	Crop	Management dates
1	Initial conditions	Ryegrass cover crop	1 Jan
	Tillage	Chisel plow 30 cm depth	1 Mar
	Tillage	Harrow-roller 5 cm depth	15 Apr
	Plant	Corn (maize)	15 Apr
	Harvest	Corn (maize)	15 Oct
	Tillage	Chisel plow 30 cm depth	15 Oct
	Plant	Ryegrass	15 Oct
2	Tillage	Chisel plow 30 cm depth	1 Mar
	Tillage	Harrow-roller 5 cm depth	15 Apr
	Plant	Soybeans	15 Apr
	Harvest	Soybeans	15 Oct
	Tillage	Chisel plow 30 cm depth	15 Oct
	Plant	Ryegrass	15 Oct

TABLE 3 Input parameters required to run the weather generator CLIGEN.

Parameter	Unit	1	2	3	4	5	6	7	8	9	10	11	12
1 Mean P	in	Mean daily precipitation per wet day for each month											
2 SD P	in	Standard deviation of Mean P per month											
3 Skew P	in	Skewness of Mean P per month											
4 Pw/w	%	Probability of a wet day following a wet day for each month											
5 Pw/d	%	Probability of a wet day following a dry day for each month											
6 TMAX AV	°F	Mean maximum temperature for each month											
7 TMIN AV	°F	Mean minimum temperature for each month											
8 SD TMAX	°F	Standard deviation of TMAX AV per month											
9 SD TMIN	°F	Standard deviation of TMIN AV per month											
10 SOLRAD	L/d ⁹	Mean solar radiation for each month											
11 SD SOL	L/d ⁹	Standard deviation of SOL RAD per month											
12 MX.5P	in	Mean maximum half hourly precipitation for each month											
13 DEW PT	°F	Mean dew point temperature for each month											
14 Time Pk	^b	Time to peak rainfall intensity											
15 % DIR ^c	%	Mean percent wind from 1 of 16 compass directions for each month											
16 MEAN	m/s ⁻¹	Mean wind speed associated with percent DIR per month											
17 SD	m/s ⁻¹	Standard deviation of MEAN per month											
18 SKEW	m/s ⁻¹	Skewness of MEAN per month											
19 CALM	%	Mean percent of days with mean wind speed <1 ms ⁻¹ per month											

Note. CLIGEN: climate generator.

^aL/d = Langley/day.

^bFor all parameters except 14, rows 1–19 represent the 12 calendar months shown along the columns.

^cPercent DIR refers to 16 different compass directions for wind direction. These are N, NNE, NE, ENE, E, ESE, SE, SSE, S, SSW, SW, WSW, W, WNW, NW, and NNW. Lines 15–18 therefore appear 16 times in a CLIGEN parameter file, meaning there are a total of 948 input values to CLIGEN (79 lines × 12).

relative humidity data were converted to dew point temperature using Equation 1 (Alduchov & Eskridge, 1996). A summary of the climatic datasets is presented in Table 4, along with details on which the CLIGEN variables these datasets were applied as follows:

$$TD = 243.04 \left(\ln \left(\frac{RH}{100} \right) + \left(\frac{17.625 * T}{243.04 + T} \right) \right) / \left(17.625 - \ln \left(\frac{RH}{100} \right) - \left(\frac{17.625 * T}{243.04 + T} \right) \right), \quad (1)$$

where TD = dew point temperature, RH = relative humidity; T = mean temperature, and LN = natural logarithm.

The CLIGEN was run for 60 years in order to drive WEPP for a 60-year simulation representing present-day baseline conditions. This duration was chosen to allow for 30 cycles of the maize-soybeans two-year crop rotation.

2.2.5 | Model validation

WEPP was validated for the study hillslope based on volumetric calculations made on sedimentation zones following a muddy flooding event on July 29, 2014. The storm that caused the muddy floods was spatially heterogeneous, with daily rainfall amounts of 31–80 mm measured at nearby rain gauges. The mean of all simulated present-day muddy flood events between 31 and 80 mm was therefore compared with the measured sedimentation to provide some indication of model performance. For further details on the event, see Mullan, Vandaele, Boardman, Meneely, and Crossley (2016).

2.3 | Future soil erosion modelling

2.3.1 | Obtaining 1.5 and 2°C GMTI scenarios

Present-day climatic conditions in CLIGEN were modified to represent future climatic conditions that correspond with (a) a 1.5°C GMTI; and (b) a 2°C GMTI. Changes in monthly-mean TMIN, TMAX, and PPT under these warmer climates were identified using projections from the CMIP5 ensemble (Taylor, Stouffer, & Meehl, 2012). For each model run, the 20-year periods during which GMTI reached 1.5 and 2°C were identified using a sliding window approach, in which running 20-year GMTI was evaluated relative to the 1986 to 2005 baseline climatology. Averaged across the HadCRUT4 (Morice, Kennedy, Rayner, & Jones, 2012), Berkeley Earth Surface Temperature (Rohde et al., 2013), and Goddard Institute for Space Studies (Hansen, Ruedy, Sato, & Lo, 2010) observational datasets, the 1986 to 2005 period was already 0.67°C warmer than preindustrial (defined as 1880–1899); GMTIs of 1.5 and 2°C were therefore identified once the models' running 20-year climates had warmed by a further 0.83 and 1.33°C, respectively. TMIN, TMAX, and PPT fields were extracted for these target climate periods, and the baseline (1986–2005), before being averaged in space over the region bounded by 5–7°E and 50–52°N. In total, this process generated 113 future scenarios with a GMTI of 1.5°C and 93 scenarios with a GMTI of 2°C.

2.3.2 | Spatial downscaling

Future climate scenarios were downscaled using a two-step approach, which first involves spatially downscaling monthly climate scenarios from GCM/ESM grid box scale to the same scale as the observed climate, followed by temporal downscaling of monthly scenarios to daily

TABLE 4 Details on climate data downloaded for Maastricht climate station, as used to parameterise CLIGEN

Variable downloaded	Temporal resolution	Time period	Station/grid	CLIGEN variables applied to
Maximum temperature	Daily	1906–2014	E-OBS	TMAX AV; SD TMAX
Minimum temperature	Daily	1906–2014	E-OBS	TMIN AV; SD TMIN
Precipitation	Daily	1957–2014	E-OBS	Mean P; SD P; Skew P; P (W/W); P (W/D)
	Sub-hourly	1957–2014	Niel-bij-Sint-Truiden	MX.5P; Time Pk
Solar radiation	Daily	1965–2014	Maastricht	SOL.RAD; SD SOL
Relative humidity	Daily	1906–2014	Maastricht	DEW PT
Wind speed	Daily	1906–2014	Maastricht	MEAN; SD; SKEW; CALM
Wind Direction	Daily	1906–2014	Maastricht	% DIR

Note. CLIGEN: climate generator.

—necessary for perturbing CLIGEN to represent future climatic conditions in WEPP. This approach has been applied in various hydrological and soil erosion modelling studies (e.g., Zhang, 2005; Zhang, Chen, Garbrecht, & Brissette, 2012; Chen, Zhang, & Brissette, 2014; Mullan, Vandaele, et al., 2016; Mullan et al., 2017). Spatial downscaling was applied using quantile mapping to bias correct the GCM/ESM data. On a monthly basis, observed TMAX, TMIN, or PPT (1986–2005) was plotted against the ranked quantiles of the hindcast period (1986–2005) GCM/ESM series using QQ-plots. In the case of TMAX and TMIN, a univariate transfer function was then fitted to each plot. In the case of PPT, a third-order polynomial function was applied to those values within the range of observations, whereas a univariate fit was applied to those outside this range. A similar approach was adopted in Zhang et al. (2012), Zhang (2016) and Mullan, Chen, and Zhang (2016). Calibrated transfer functions were then applied to the future 20-year GCM/ESM timeslice.

2.3.3 | Temporal downscaling

The spatially downscaled climate scenarios needed to be temporally downscaled to daily scenarios to drive CLIGEN. In theory, any of the 948 input values in Table 3 can be modified to represent changed climatic conditions. Table 5 shows that CLIGEN parameters were modified and how they were modified. Transitional probabilities (Pw/w and Pw/d) were calculated by first splitting historical precipitation into three groups—wet months, dry months, and all months. Wet months were calculated as those where monthly precipitation totals equal or exceed the 90th percentile of the mean monthly precipitation totals over the entire 1986 to 2005 period for each respective month. Dry months were classified as the months that do not fulfil this criterion. Linear relationships were then developed between historical total monthly precipitation and the transitional probabilities for each of these three groups, with future transitional probabilities, then calculated by forcing these transfer functions with future monthly precipitation totals. In order to preserve the projected mean monthly precipitation totals (R_m) following the adjustment of transitional probabilities, Mean P was calculated using the approach of Zhang, Nearing, Garbrecht, and Steiner (2004) and Zhang et al. (2012). First, the unconditional probability of precipitation occurrence (π) was calculated as follows:

TABLE 5 How CLIGEN parameters were modified to account for changed climatic conditions. Each case of a variable versus another variable refers to developing linear relationships between those variables using the 1986 to 2005 historical data on a monthly basis

CLIGEN parameter	How was it modified?
Mean P	Equations 3 and 4
SD P	Mean P vs SD P—forced with future Mean P
SKEW P	Q99 vs SKEW P—forced with future Q99 (itself calculated based on linear relationships between historical Q99 and SD P and forced with future SD P)
P(W/W)	See next paragraph
P(W/D)	See next paragraph
TMAX AV	Adjusted directly from future TMAX AV
TMIN AV	Adjusted directly from future TMIN AV
SD TMAX	TMAX AV vs SD TMAX—forced with future TMAX AV
SD TMIN	TMAX AV vs SD TMAX—forced with future TMAX AV
SOL.RAD	TMAX AV vs SOL.RAD—forced with future TMAX AV
SD.SOL	TMAX AV vs SD.SOL—forced with future TMAX AV
MX.5P	TMIN AV vs SOL.RAD (exponential function)— forced with future TMIN AV
DEW PT	TMAX AV vs DEW PT—forced with future TMAX AV

$$\pi = \frac{Pw/d}{1 + \frac{Pw}{d} - Pw/d}, \quad (2)$$

the new Mean P is then calculated using:

$$Mean P = \frac{R_m}{N_d \pi} \quad (3)$$

where Mean P and R_m are as described before, and $N_d \pi$ is the expected number of wet days in the month.

2.3.4 | Running WEPP under future scenarios

WEPP was run for the future by holding the slope, soil, and management input files constant from the present-day simulation and perturbing the climate file under the various downscaled climate scenarios for 60-year time periods, as was the case for present-day baseline modelling. Future muddy flooding diagnostics outputted by WEPP include mean annual

precipitation, mean annual runoff, mean annual soil loss, and mean annual sediment yield. These statistics are taken as an annual average across the entire hillslope, with the exception of sediment yield—this is the amount of sediment that leaves the hillslope and enters the wider environment. Other analysed outputs include mean maximum monthly precipitation—the mean (across all years of the record) of the highest daily precipitation amount for each respective month. For simplicity, this is hereafter referred to as rainfall intensity. Return periods (RP) for all simulated sediment yield and rainfall intensity events under present-day conditions and under the mean and maximum of future 1.5 and 2°C scenarios were computed by using:

$$RP = \frac{n + 1}{m}, \quad (4)$$

where n represents the number of years in the record and m is the number of recorded occurrences of each event.

Testing for statistically significant differences in muddy flooding metrics between (a) observed and 1.5°C scenarios, (b) observed and 2°C scenarios, and (c) 1.5 and 2°C scenarios, was conducted using the Mann–Whitney U tests. Data were first tested for normality using the Anderson–Darling tests and were found to be not normally distributed, meaning nonparametric statistical testing needed to be completed. The Mann–Whitney U tests compare whether two samples means come from the same population. Tests were conducted on annual means of precipitation and sediment yield across all 1.5°C ($n = 113$) and 2°C scenarios ($n = 93$), monthly means and maxima of all observed, 1.5 and 2°C scenarios ($n = 12$ for all), and the return period means and maxima of all observed, 1.5 and 2°C scenarios ($n = 39$ for all). Results are reported in Table 7 in the form of p values less than 0.05 (statistically significant at > 95% confidence level), and less than 0.005 (statistically significant at > 99.5% confidence level).

3 | RESULTS

3.1 | Model performance

The measured sedimentation zone following a muddy flood event on July 29, 2014 at Kluiskepel hillslope was 12 t ha⁻¹, which compares reasonably closely to the simulated mean of soil eroded for present-day events of a similar magnitude, which is 16.2 t ha⁻¹. Because not all eroded soil would be deposited in the sedimentation zone, the measured figure of 12 t ha⁻¹ should represent an underestimate of the total amount of soil eroded (Mullan, Vandaele, et al., 2016), giving further confidence to simulated rates that are ~33% higher. Of course, it is recognised that validation based on a single event is less than ideal, but is much better than having nothing to compare simulations with.

3.2 | Mean annual changes

Table 6 shows the absolute and relative changes in mean annual muddy flooding diagnostics across all future 1.5 and 2°C GMTI climate scenarios compared with the present-day baseline. Increases in all muddy flooding diagnostics are projected when the mean of all 2 and 1.5°C scenarios are compared with the present-day baseline, with

TABLE 6 Present-day baseline and future simulated mean annual rates of muddy flooding diagnostics

Diagnostic/scenario	Precipitation (mm)	Runoff (mm)	Soil loss (t ha ⁻¹)	Sediment yield (t ha ⁻¹)
Baseline	735	5.4	6.9	2.3
1.5°C	773	6.0	7.6	2.5
Change	+5%	+11%	+10%	+10%
2°C	779	6.6	8.0	2.8
Change	+6%	+21%	+16%	+22%

larger increases in 2°C scenarios for all diagnostics. Figure 2 shows the full distribution of projected changes in the same diagnostics for Kluiskepel hillslope under the same scenarios. The median across all scenarios for both 1.5 and 2°C is very close to the present-day baseline for runoff, soil loss, and sediment yield, but is notably higher than the baseline in the case of precipitation. For runoff, soil loss, and sediment yield, the upper extremes are higher for 1.5°C scenarios compared with 2°C scenarios. As shown in Table 7, there is no statistically significant difference between mean annual changes in muddy flooding metrics for 1.5 versus 2°C.

3.3 | Seasonal changes

Figure 3 shows projected changes in rainfall totals, rainfall intensity, and sediment yield for each month of the year across all 1.5 and 2°C scenarios, with planting and harvest dates also shown. In terms of sediment yield, the model mean is higher than the baseline during June, July, and October, and is lower during May, August, and September. The model mean for rainfall totals is higher than the baseline every month of the year, except for June in the case of 1.5°C, and June and September for 2°C. The model mean for rainfall intensity is typically higher than the baseline during most of the year under both scenarios, except for August and September. For all three muddy flooding diagnostics, the extreme increases occur during the summer months—particularly in July. As shown in Table 7, observed versus future monthly muddy flooding metrics are only statistically significant for the maximum future scenarios—not the means.

3.4 | Muddy flood events

Figure 4 shows return periods for rainfall during individual muddy flooding events and sediment yield during muddy flood events for the present-day baseline, as well as the mean and maximum of all 1.5 versus 2°C scenarios. The mean of all future scenarios for both rainfall and sediment yield reveals an increase in the magnitude of events for a given return period up to 1 in 30 years, but it shows lower magnitude responses for the longest return period of 1 in 61 years. The maximum of all future scenarios reveals markedly higher magnitude events for all given return periods. For example, the 1 in 61 year event for sediment yield for the present-day baseline is 40 t/ha, compared with 96 t/ha for the maximum 1.5°C scenario and 60 t/ha for the maximum 2°C scenario. The number of muddy flood events is also projected to increase—from 3.8 events per year in the present-day to 4.4 and 4.8 events per year under the mean of all 1.5 versus 2°C scenarios respectively. As

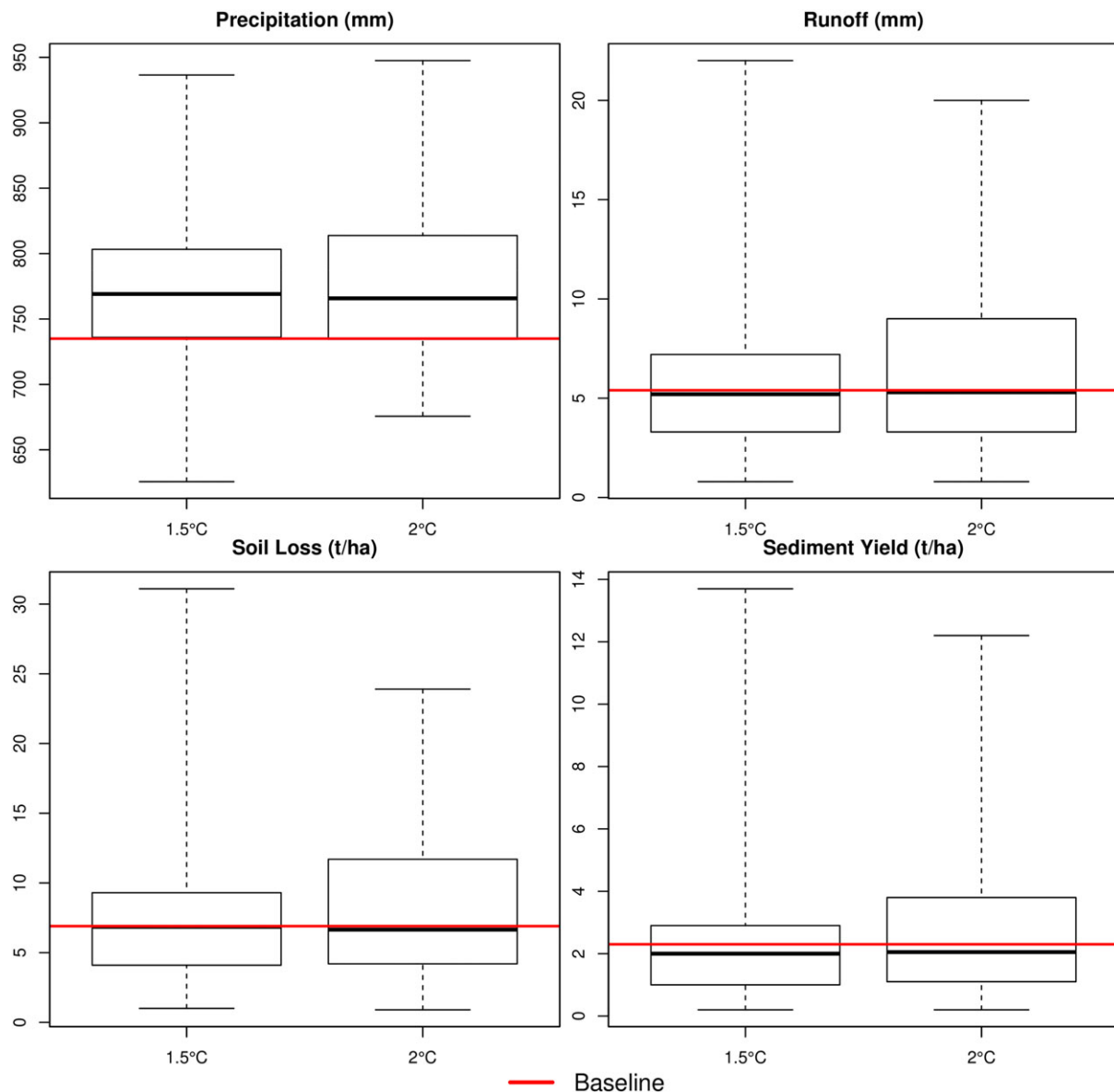


FIGURE 2 Full distribution of future annual simulated rates of muddy flooding diagnostics for all 1.5 and 2°C scenarios compared with present-day baseline rates (red) [Colour figure can be viewed at wileyonlinelibrary.com]

TABLE 7 Results from Mann–Whitney U tests conducted independently on muddy flooding metrics for present-day (OBS) versus 1.5°C scenarios, OBS versus 2°C scenarios, and 1.5 versus 2°C scenarios. Dashes (–) represent no statistically significant changes

Diagnostic/ scenario	Precipitation			Sediment yield		
	OBS vs. 1.5°C	OBS vs. 2°C	1.5 vs. 2°C	OBS vs. 1.5 °C	OBS vs. 2°C	1.5 vs. 2°C
Annual means	N/A	N/A	–	N/A	N/A	–
Monthly means	–	–	–	–	–	–
Monthly maxima	$p < 0.005$	$p < 0.005$	–	$p < 0.005$	$p < 0.005$	–
Return period means	$p < 0.05$	$p < 0.05$	–	$p < 0.05$	$p < 0.05$	–
Return period maxima	$p < 0.005$	$p < 0.005$	–	$p < 0.005$	$p < 0.005$	–

shown in Table 7, differences between observed return periods for precipitation and sediment yield versus return periods for the mean of 1.5 and 2°C scenarios, respectively, are both statistically significant at a 95% confidence level. When observed return periods are compared with return periods for the maximum of the two sets of future scenarios independently, statistically significant differences at a 99.5% confidence level are noted.

4 | DISCUSSION

4.1 | Present-day muddy flooding

Present-day muddy flood events are concentrated in August and September because of two related factors: (a) the detachment of soil particles between the widely spaced rows of maize plants (Vogel,

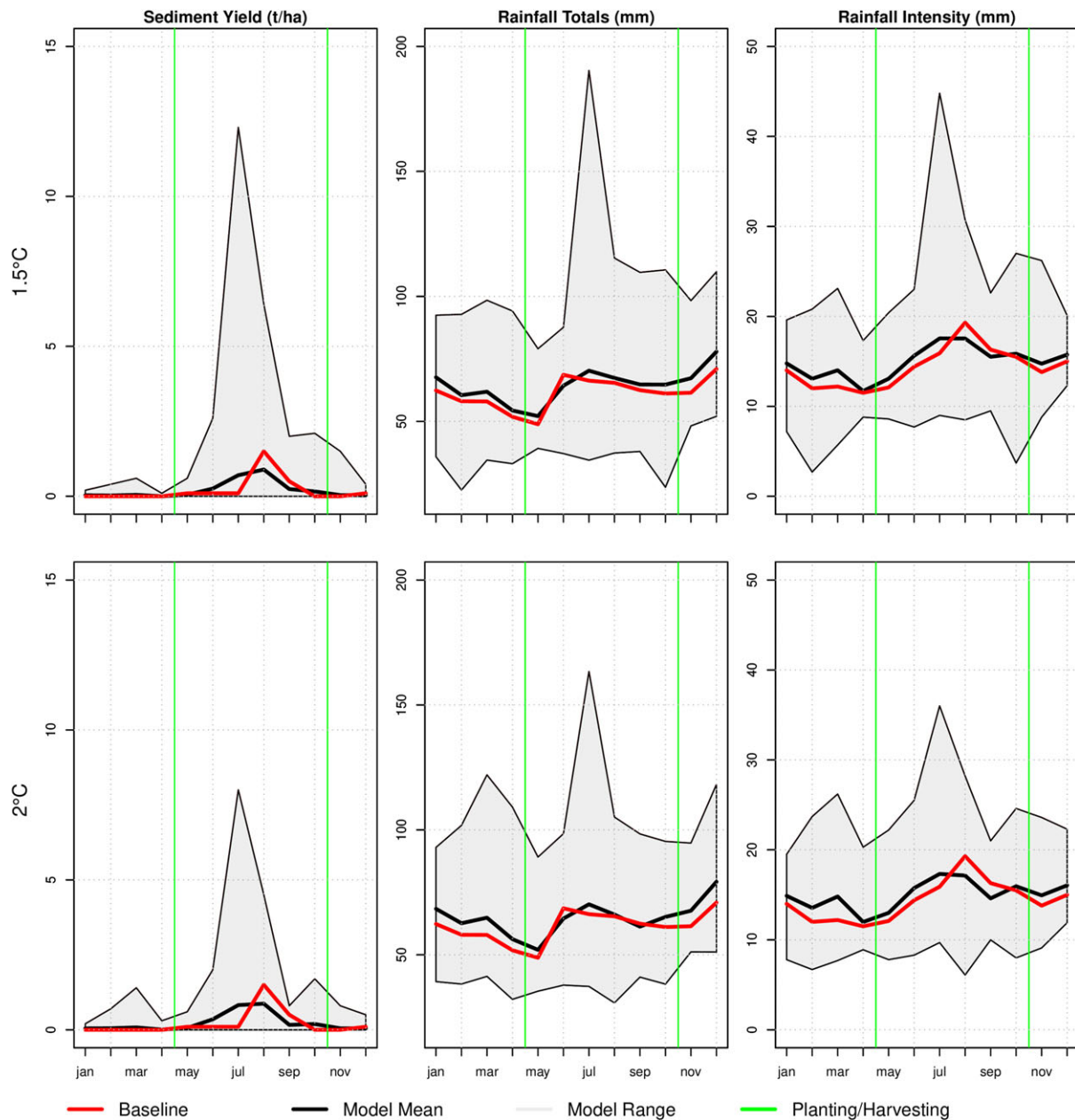


FIGURE 3 Full distribution of future monthly simulated rates of muddy flooding diagnostics for all 1.5 and 2°C scenarios compared with present-day baseline rates (red) [Colour figure can be viewed at wileyonlinelibrary.com]

Deumlich, & Kaupenjohann, 2016) from planting in mid-April to harvest in mid-October; and (b) maximum rainfall intensity during August and September. Present-day monthly rainfall totals peak in mid-winter and early summer, so it is clear that rainfall intensity rather than rainfall totals exerts a dominant control on muddy flooding in this region. This is unsurprising, because soil erosion and muddy flood events in Limburg are triggered by the detachment of silty soils following intense short-lived thunderstorms (Evrard, Bielanders, et al., 2007). Intense rainfall through raindrop impact initiates processes such as slaking of aggregates, microcracking, and physicochemical dispersion (Bresson & Boiffin, 1990), leading to the formation of a surface crust by local rearrangement of particles, and then a depositional crust when particles are transported and deposited further away (Valentin & Bresson, 1992). Surface crusts

greatly reduce the infiltration capacity as well as soil surface roughness—which, along with vegetation cover—are the most important field factors for the generation of runoff and erosion (Le Bissonnais, 1996). It is therefore unsurprising that the highest rainfall intensity during August and September produces virtually all of the annual sediment yield during these same 2 months.

4.2 | Future muddy flooding

As shown in the results section, the evidence for future increases in soil erosion and muddy flooding is mixed. It is generally only the maximum of the future scenarios, which shows statistically significant changes from the present-day, owing to the extreme nature of the

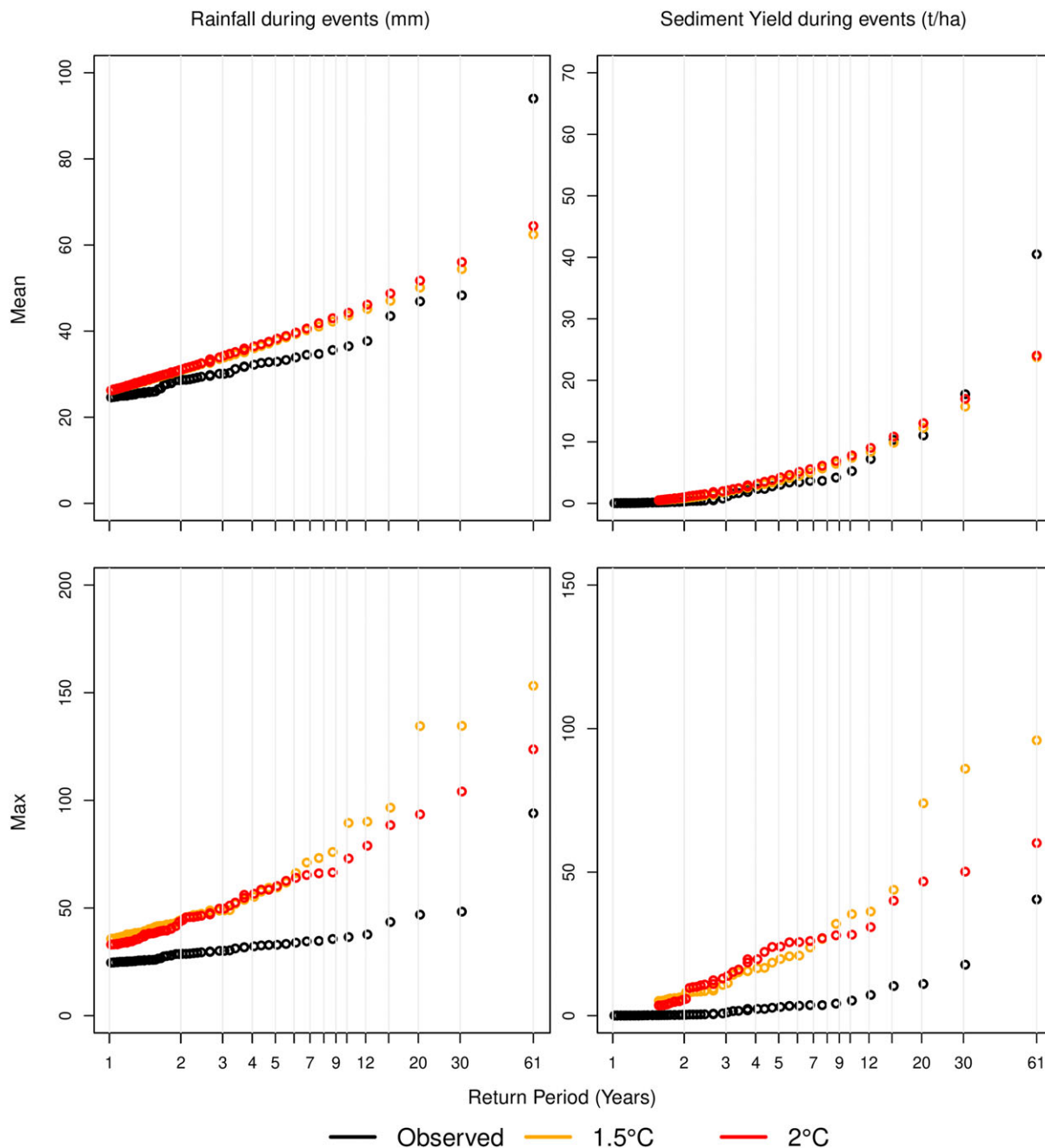


FIGURE 4 Return periods for rainfall during muddy flood events (left panels) and sediment yield during muddy flood events (right panels) for the present-day baseline, as well as the mean and maximum of all 1.5 and 2°C future scenarios [Colour figure can be viewed at [wileyonlinelibrary.com](https://onlinelibrary.wiley.com)]

future scenarios with highest rainfall totals and intensity. The main reason we see little statistically significant change in the mean of the future scenarios is because (a) it has been assumed that land use remains unchanged; and (b) the magnitude and timing of rainfall intensity is not markedly different from the present-day. Peak sediment yield is projected to remain in August in the future, but is very closely followed by July—a month with very little sediment yield at the present-day. Overall, the projections in Figure 3 show an earlier and longer muddy flooding season in the future. The reason for this shift in timing is simple—it reflects the changing seasonality of rainfall intensity, which clearly remains the dominant external climatic control on future muddy flooding above monthly rainfall totals. We can see

this influence clearly in Figure 5, where the correlation between sediment yield and rainfall intensity is much stronger than the correlation between sediment yield and rainfall totals, both at the present-day and in the future. This was shown to be the case for the same hillslope in Mullan, Vandaele, et al. (2016). Unlike present-day muddy flooding, the earlier and extended future muddy flooding season means that sediment yield would likely be generated more extensively across the width of the field, both between and within rows of maize. Since maize takes ~8–10 weeks to establish, a sufficient protective cover to the soil to prevent detachment following planting (Boardman, 2010; though this may change in the future with declining maize yields, e.g., Challinor, Koehler, Ramirez-Villegas, Whitfield, and Das

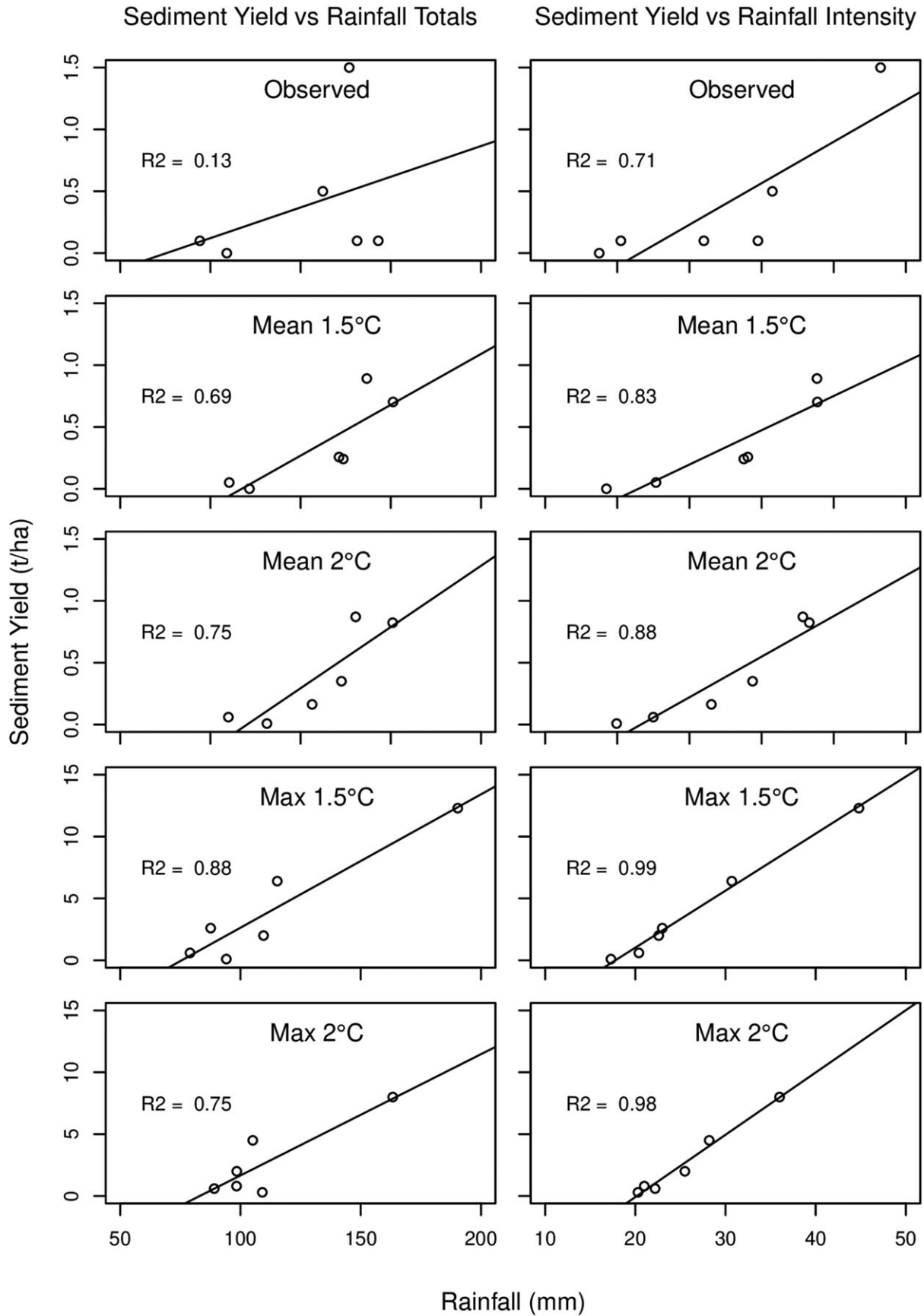


FIGURE 5 Correlation between sediment yield and rainfall totals (left panels) and sediment yield and rainfall intensity (right panels) during the six key months for muddy flooding (April–September). Panels labelled Mean refer to the mean of all 1.5 or 2°C scenarios, whereas Max represents the maximum of these scenarios

(2016)), it is very feasible that much of the muddy flooding from May–July would be generated from rill formation across rows of maize plants, whereas muddy flooding later in the year would follow present-day patterns between rows (Vogel et al., 2016). The longer future muddy flooding season also helps explain why the magnitude of rainfall amounts and sediment yield during muddy flood events for the model mean are projected to increase for return periods up to 30 years, but decrease for the longest return period of 61 years. This reflects the fact that more muddy flood events are projected in the future over a longer time period, but that no single month will produce rainfall intensity and consequently sediment yield as high as August does at the present-day. It should be pointed out, however, that the maximum future scenario projects large increases in the magnitude of events for all return periods, illustrating the potential for larger-scale muddy flood events in the future.

4.3 | Difference between 1.5 and 2°C

The difference in muddy flooding diagnostics for 1.5 versus 2°C GMTI is minimal for most metrics analysed, with no statistically significant differences for any metrics (Table 7). Both the mean and median of all future scenarios lie near present-day baseline rates for all diagnostics. This simply reflects an averaging of many future climate scenarios incorporating both higher and lower rainfall rates than present day. What is most interesting is the change in extremes, where very large increases in rainfall, runoff, soil loss, and sediment yield are projected for both 1.5 and 2°C future scenarios—but most dramatically for the former. With the promotion of a more vigorous hydrological cycle under increased warming (Hartmann et al., 2013), it may seem surprising that the extra 0.5°C warming under 2°C scenarios fails to result in consistently higher magnitude muddy flooding than 1.5°C scenarios. The most likely explanation relates to the timing of changing rainfall characteristics under 1.5 versus 2°C scenarios. Figure 3 reveals higher rainfall totals and intensity, and consequently higher sediment yield, during the winter and spring months for 2°C scenarios—both in terms of the mean and extremes. Crucially though, it is the summer months when the damage is done—and this is when rainfall totals and intensity are projected to be higher under 1.5°C scenarios versus 2°C scenarios. This could possibly relate to a tendency for many climate models to project wetter winters and drier summers with increased warming—a trend clearly seen in recent decades in midlatitude continental regions (Trenberth & Shea, 2005). Alternatively, it could relate to climate models capturing complex changes in atmospheric circulation and a shift in the storm track, resulting in a high degree of spatial and temporal variability in rainfall characteristics (Trenberth, 2011). Regardless of the causal mechanisms, what is clear is that the timing of rainfall intensity is the most important factor in terms of whether 1.5 or 2°C scenarios impact soil erosion and muddy flooding more. The role of timing with respect to rainfall characteristics and land cover is a well-known cause of soil erosion and muddy flooding and has been reported previously for the same hillslope (Mullan, Vandaele, et al., 2016). For a more in-depth

discussion of timing with respect to soil erosion, see Boardman and Favis-Mortlock (2014), and Burt, Boardman, Foster, and Howden (2015).

4.4 | Implications for future mitigation

Uncertainty was reported by Moser (2010) as one of the key reasons for inaction with climate adaptation and mitigation. Because progress has been made with mitigating muddy flooding in Flanders since the adoption of the Erosion Decree in 2001, it is important that decision-makers are not complacent about the new challenges imposed by climate change and that mitigation measures are continually adapted to make them resilient to climate change. Given the uncertainty imposed by the many scenarios presented here (206), low-regret, flexible, and 'soft solutions' (Wilby & Dessai, 2010) are best placed as adaptation options. This may include widening grass buffer strips and grass waterways or increasing the capacity of retention ponds to accommodate increased runoff and sediment yield. Such measures have already been shown to be successful and cost-effective within existing policy structures (e.g., Evrard, Persoons, et al., 2007), so adapting these mitigation measures seems the most pragmatic way to ensure muddy flooding mitigation remains resilient to future climate change.

4.5 | Limitations and future research

Crop rotations and dates of farming operations were left unchanged for future WEPP simulations. However, it is acknowledged that to project the full range of impacts of climate change on soil erosion and muddy flooding, changes in land cover and farming dates need to be accounted for. In fact, changing land use has been shown in many instances to be the dominant factor in driving increases in soil erosion (e.g., Boardman & Vandaele, 2015; Mullan, 2013a, 2013b; Mullan, Favis-Mortlock, & Fealy, 2012; O'Neal, Nearing, Vining, Southworth, & Pfeifer, 2005). This is unsurprising given that different crops have varying susceptibilities to muddy flooding, owing to differences in time taken to establish crop cover, canopy height, plant spacing within rows etc. Different crops and modified dates of planting and/or harvest also have the potential to modify the soil surface conditions, for example, timing of crust development—which is fundamental to the timing and magnitude of muddy flooding. For example, within the Belgian loess belt, Evrard, Persoons, et al. (2007) found that rainfall amounts of 46 ± 20 mm are needed to trigger muddy floods from July–September, but only 25 ± 12 mm is needed from May–June. Some previous studies (e.g., O'Neal et al., 2005; Zhang & Nearing, 2005; Mullan, Favis-Mortlock, & Fealy, 2012; Mullan, 2013a, 2013b) have used scenarios-based approaches to changing crop types, with some also modifying dates of planting and/or harvest based on changes in temperature and growing season. The reason we did not account for these changes is because of the associated problems, including the dependence on wider socioeconomic factors such as, change in demographics, and economic subsidies as well as the fact that changes in farming dates depend on other complex physical (e.g., field conditions driven by temperature, rainfall, evapotranspiration, and drainage) and socioeconomic (e.g., availability of labour, and

cultural norms) factors. Future studies (whose aim encompasses the direct and indirect impacts of climate change on muddy flooding) should explore novel ways to ensure crop type and dates of farming operation are examined along with the direct impacts of climate change. Another limitation with this study is the scale. Projected rates of muddy flooding have been made for one hillslope in Flanders. Larger projects would need to target whole catchments rather than individual hillslopes, especially considering the hydrological connectivity of these landscapes (Boardman & Vandaele, 2015). The study also fails to address the spatial patterns of sediment yield and the relative contribution of sediment from rills, gullies, and interrill areas. Although a wide number of climate scenarios were used here, the choice of spatial and temporal downscaling techniques can considerably impact the resultant projections (e.g., Mullan, Fealy, & Favis-Mortlock, 2012). Finally, the lack of measured data to validate modelled projections is a limitation. Regular monitoring across hillslopes and catchments needs to be conducted to construct databases to help more fully ascertain the extent of the problem in the present day, as well as assist in model development.

5 | CONCLUSIONS

- No statistically significant differences exist when any of the average annual or monthly metrics of soil erosion and muddy flooding are compared between the present-day and the mean for the two sets of future scenarios.
- Statistically significant differences exist when present-day return periods are compared with return periods for the mean of both sets of future scenarios, whereas statistical significance is also evident with present-day versus all metrics for the maximum of the two sets of future scenarios.
- Subtle changes in the seasonality of future muddy flooding are projected, revealing an earlier and longer muddy flooding season with more events spread across a longer period over the summer months.
- No statistically significant differences exist when any of the average annual, monthly or event-based metrics of soil erosion and muddy flooding are compared between 1.5 and 2°C future scenarios.
- Soil erosion and muddy flooding (as impacted directly by climatic changes) are therefore not particularly sensitive to small changes in GMTI—at least for this case study site. It is a changes in the timing of rainfall characteristics that are fundamental—and these do not always follow clear patterns with increased warming.
- Regardless of the magnitude of future warming, there is evidence here to suggest changes in the magnitude and timing of muddy flooding in the future could increase the scale of the problem. Future studies that examine the indirect impact of changing crop type and dates of farming operations are needed to more fully investigate this problem. Regardless of this, it is clear that decision-makers should continually adapt muddy flooding mitigation measures within existing policy frameworks to ensure they remain resilient to future climate change.

ACKNOWLEDGMENTS

The authors thank the British Society for Geomorphology, who provided an early career research grant to the lead author that helped with the execution of this study.

ORCID

Donal Mullan  <http://orcid.org/0000-0002-6363-3150>

REFERENCES

- Alduchov, O. A., & Eskridge, R. E. (1996). Improved magnus form approximation of saturation vapor pressure. *Journal of Applied Meteorology*, 35, 601–609. [https://doi.org/10.1175/1520-0450\(1996\)035<0601:IMFAOS>2.0.CO;2](https://doi.org/10.1175/1520-0450(1996)035<0601:IMFAOS>2.0.CO;2)
- Biielders, C. L., Ramelot, C., & Persoons, E. (2003). Farmer perception of runoff and erosion and extent of flooding in the silt-loam belt of the Belgian Walloon Region. *Environmental Science and Policy*, 6, 85–93. [https://doi.org/10.1016/S1462-9011\(02\)00117-X](https://doi.org/10.1016/S1462-9011(02)00117-X)
- Boardman, J. (2010). A short history of muddy floods. *Land Degradation and Development*, 21, 303–309. <https://doi.org/10.1002/ldr.1007>
- Boardman, J., & Favis-Mortlock, D. T. (2014). The significance of drilling date and crop cover with reference to soil erosion by water, with implications for mitigating erosion on agricultural land in South East England. *Soil Use and Management*, 30, 40–47. <https://doi.org/10.1111/sum.12095>
- Boardman, J., Ligneau, L., De Roo, A., & Vandaele, K. (1994). Flooding of property by runoff from agricultural land in northwestern Europe. *Geomorphology*, 10, 183–196. [https://doi.org/10.1016/0169-555X\(94\)90016-7](https://doi.org/10.1016/0169-555X(94)90016-7)
- Boardman, J., & Vandaele, K. (2015). Effect of the spatial organization of land use on muddy flooding from cultivated catchments and recommendations for the adoption of control measures. *Earth Surface Processes and Landforms*, 41, 336–343. <https://doi.org/10.1002/esp.3793>
- Boardman, J., Verstraeten, G., & Biielders, C. (2006). Muddy floods. In J. Boardman, & J. Poesen (Eds.), *Soil Erosion in Europe* (pp. 743–755). Chichester: Wiley. <https://doi.org/10.1002/0470859202.ch53>
- Bresson, L.-M., & Boiffin, J. (1990). Morphological characterisation of soil crust development stages on an experimental field. *Geoderma*, 47, 301–325. [https://doi.org/10.1016/0016-7061\(90\)90035-8](https://doi.org/10.1016/0016-7061(90)90035-8)
- Burt, T., Boardman, J., Foster, I., & Howden, N. (2015). More rain, less soil: Long-term changes in rainfall intensity with climate change. *Earth Surface Processes and Landforms*, 41, 563–566. <https://doi.org/10.1002/esp.3868>
- Challinor, A. J., Koehler, A.-K., Ramirez-Villegas, J., Whitfield, S., & Das, B. (2016). Current warming will reduce yields unless maize breeding and seed systems adapt immediately. *Nature Climate Change*, 6, 954–958. <https://doi.org/10.1038/NCLIMATE3061>
- Chen, J., Zhang, X. C., & Brissette, F. P. (2014). Assessing scale effects for statistically downscaling precipitation with GPCP model. *International Journal of Climatology*, 34, 708–727. <https://doi.org/10.1002/joc.3717>
- Evrard, O., Biielders, C. L., Vandaele, K., & van Wesemael, B. (2007). Spatial and temporal variation of muddy floods in central Belgium, off-site impacts and potential control measures. *Catena*, 70, 443–454. <https://doi.org/10.1016/j.catena.2006.11.011>
- Evrard, O., Heitz, C., Liégeois, M., Boardman, J., Vandaele, K., Auzet, A.-V., & van Wesemael, B. (2010). A comparison of management approaches to control muddy floods in central Belgium, northern France and southern England. *Land Degradation & Development*, 21, 1–14. <https://doi.org/10.1002/ldr.1006>
- Evrard, O., Persoons, E., Vandaele, K., & van Wesemael, B. (2007). Effectiveness of erosion mitigation measures to prevent muddy floods: A case study in the Belgian loam belt. *Agriculture, Ecosystems and Environment*, 118, 149–158. <https://doi.org/10.1016/j.agee.2006.02.019>

- Flanagan, D. C., & Livingston, S. J. (1995). USDA-Water Erosion Prediction Project (WEPP) User Summary. NSERL Report No.11. IN., USA: West Lafayette.
- Flanagan, D. C., & Nearing, M. A. (1995). USDA-Water Erosion Prediction Project (WEPP) Hillslope profile and watershed model documentation. NSERL Report No.10. IN., USA: West Lafayette.
- Govers, G., Merckx, R., van Wesemael, B., & van Oost, K. (2017). Soil conservation in the 21st century: Why we need smart agricultural intensification. *The Soil*, 3, 45–49. <https://doi.org/10.5194/soil-3-45-2017>
- Hansen, J., Ruedy, R., Sato, M., & Lo, K. (2010). Global surface temperature change. *Reviews of Geophysics*, 48, RG4004. <https://doi.org/10.1029/2010RG000345>
- Hartmann, D. L., Klein Tank, A. M. G., Rusticucci, M., Alexander, L. V., Brönnimann, S., Charabi, Y., ... Zhai, P. M. (2013). Observations: Atmosphere and Surface. In T. Stocker, D. Qin, G.-K. Plattner, M. Tignor, S. Allen, J. Boschung, et al. (Eds.), *Climate change 2013: The physical science basis. Contribution of working group I to the fifth assessment report of the intergovernmental panel on climate change* (pp. 1–100). Cambridge, UK, and New York, NY, USA: Cambridge University Press. <https://doi.org/10.1017/CBO9781107415324.004>
- Haylock, M. R., Hofstra, N., Klein Tank, A. M. G., Klok, E. J., Jones, P. D., & New, M. (2008). A European daily high-resolution gridded dataset of surface temperature and precipitation. *Journal of Geophysical Research-Atmospheres*, 113, D20119. <https://doi.org/10.1029/2008JD010201>
- IPCC (2013). Summary for Policymakers. In T. Stocker, D. Qin, G.-K. Plattner, M. Tignor, S. Allen, J. Boschung, et al. (Eds.), *Climate change 2013: The physical science basis. Contribution of working group I to the fifth assessment report of the intergovernmental panel on climate change* (pp. 1–100). Cambridge, UK, and New York, NY, USA: Cambridge University Press. <https://doi.org/10.1017/CBO9781107415324.004>
- James, R., Otto, F., Parker, H., Boyd, E., Cornforth, R., Mitchell, D., & Allen, M. (2015). Characterising loss and damage from climate change. *Nature Climate Change*, 4, 1221–1238. <https://doi.org/10.1038/nclimate2411>
- Le Bissonnais, Y. (1996). Aggregate stability and assessment of soil crustability and erodibility: I. Theory and methodology. *European Journal of Soil Science*, 47, 425–437. <https://doi.org/10.1111/j.1365-2389.1996.tb01843.x>
- Lenderink, G., & van Meijgaard, E. (2008). Increase in hourly precipitation extremes beyond expectations from temperature changes. *Nature Geoscience*, 1, 511–514. <https://doi.org/10.1038/ngeo262>
- Li, Z., & Fang, H. (2016). Impacts of climate change on water erosion: A review. *Earth Science Reviews*, 163, 94–117. <https://doi.org/10.1016/j.earscirev.2016.10.004>
- Morice, C. P., Kennedy, J. J., Rayner, N. A., & Jones, P. D. (2012). Quantifying uncertainties in global and regional temperature change using an ensemble of observational estimates: The HadCRUT4 data set. *Journal of Geophysical Research-Atmospheres*, 117, D080101. <https://doi.org/10.1029/2011JD017187>
- Moser, S. C. (2010). Communicating climate change: History, challenges, process and future directions. *WIREs Climate Change*, 1, 31–53. <https://doi.org/10.1002/wcc.11>
- Mullan, D. J. (2013a). Soil erosion on agricultural land in the north of Ireland: Past, present and future potential. *Irish Geography*, 45, 154–171. <https://doi.org/10.1080/00750778.2013.776216>
- Mullan, D. J. (2013b). Soil erosion under the impacts of future climate change: Assessing the statistical significance of future changes and the potential on-site and off-site problems. *Catena*, 109, 234–246. <https://doi.org/10.1016/j.catena.2013.03.007>
- Mullan, D. J., Chen, J., & Zhang, X. C. (2016). Validation of non-stationary precipitation series for site-specific impact assessment: Comparison of two statistical downscaling techniques. *Climate Dynamics*, 46, 967–986. <https://doi.org/10.1007/s00382-015-2626-x>
- Mullan, D. J., Favis-Mortlock, D. T., & Fealy, R. (2012). Addressing key limitations associated with modelling soil erosion under the impacts of future climate change. *Agricultural and Forest Meteorology*, 156, 18–30. <https://doi.org/10.1016/j.agrformet.2011.12.004>
- Mullan, D. J., Fealy, R., & Favis-Mortlock, D. T. (2012). Developing site-specific future temperature scenarios for Northern Ireland: Addressing key issues employing a statistical downscaling approach. *International Journal of Climatology*, 32, 2007–2019. <https://doi.org/10.1002/joc.2414>
- Mullan, D. J., Swindles, G., Patterson, T., Galloway, J., Macumber, A., Falck, H., ... Pisaric, M. (2017). Climate change and the long-term viability of the world's busiest heavy-haul ice road. *Theoretical and Applied Climatology*, 129, 1089–1108. <https://doi.org/10.1007/s00704-016-1830-x>
- Mullan, D. J., Vandaele, K., Boardman, J., Meneely, J., & Crossley, L. H. (2016). Modelling the effectiveness of grass buffer strips in managing muddy floods under a changing climate. *Geomorphology*, 270, 102–120. <https://doi.org/10.1016/j.geomorph.2016.07.012>
- New, M., Liverman, D., Schroeder, H., & Anderson, K. (2011). Four degrees and beyond: the potential for a global temperature increase of four degrees and its implications. *Philosophical Transactions of the Royal Society A: Mathematical, Physical and Engineering Sciences*, 369, 6–19. <https://doi.org/10.1098/rsta.2010.0303>
- Nicks, A. D., Lane, L. J., & Gander, G. A. (1995). Weather Generator, in: Flanagan, D. C., & Nearing, M. A. (Eds.), Hillslope profile and watershed model documentation. NSERL Report No.10. IN., USA: West Lafayette.
- O'Neal, M. R., Nearing, M. A., Vining, R. C., Southworth, J., & Pfeifer, R. A. (2005). Climate change impacts on soil erosion in Midwest United States with changes in crop management. *Catena*, 61, 165–184. <https://doi.org/10.1016/j.catena.2005.03.003>
- Pimentel, D. (2006). Soil erosion: A food and environmental threat. *Environment, Development and Sustainability*, 8, 119–137. <https://doi.org/10.1007/s10668-005-1262-8>
- Rohde, R., Muller, R. A., Jacobsen, R., Muller, E., Perlmutter, S., Rosenfeld, A., ... Wickham, C. (2013). A new estimate of the average Earth surface land temperature spanning 1753 to 2011. *Geoinformatics and Geostatistics: An Overview*, 1, 1000101. <https://doi.org/10.4172/2327-4581.1000101>
- Statistics Belgium (2006). Retrieved from <http://www.statbel.fgov.be>.
- Sun, Y., Solomon, S., Dai, A., & Portmann, R. (2007). How often will it rain? *Journal of Climate*, 79, 185–211. <https://doi.org/10.1175/JCLI4263.1>
- Taylor, K. E., Stouffer, R. J., & Meehl, G. A. (2012). An overview of CMIP5 and the experiment design. *Bulletin of the American Meteorological Society*, 93, 485–498. <https://doi.org/10.1175/BAMS-D-11-00094.1>
- Trenberth, K. E. (2011). Changes in precipitation with climate change. *Climate Research*, 47, 123–138. <https://doi.org/10.3354/cr00953>
- Trenberth, K. E., & Shea, D. J. (2005). Relationships between precipitation and surface temperature. *Geophysical Research Letters*, 32, L14703. <https://doi.org/10.1029/2005GL022760>
- UNFCCC (2015). Decision 1/CP.21. The Paris Agreement. Retrieved from https://unfccc.int/sites/default/files/english_paris_agreement.pdf
- Valentin, C., & Bresson, L.-M. (1992). Morphology, genesis and classification of surface crusts in loamy and sandy soils. *Geoderma*, 55, 225–245. [https://doi.org/10.1016/0016-7061\(92\)90085-L](https://doi.org/10.1016/0016-7061(92)90085-L)
- Verstraeten, G., Poesen, J., Goossens, D., Gillijns, K., Bielders, C., Gabriels, D., ... Govers, G. (2006). Belgium. In J. Boardman, & J. Poesen (Eds.), *Soil Erosion in Europe* (pp. 384–411). Chichester: Wiley. <https://doi.org/10.1002/0470859202.ch30>
- Vogel, E., Deumlich, D., & Kaupenjohann, M. (2016). Bioenergy maize and soil erosion—risk assessment and erosion control concepts. *Geoderma*, 261, 80–92. <https://doi.org/10.1016/j.geoderma.2015.06.020>
- Wilby, R. L., & Dessai, S. (2010). Robust adaptation to climate change. *Weather*, 65, 180–185. <https://doi.org/10.1002/wea.543>
- World Reference Base (2014) World reference base for soil resources 2014. Retrieved from <http://www.fao.org/3/i3794en/i3794en.pdf>
- Yang, D., Kanae, S., Oki, T., Koike, T., & Musiak, K. (2003). Global potential soil erosion with reference to land use and climate changes. *Hydrological Processes*, 17, 2913–2928. <https://doi.org/10.1002/hyp.1441>

- Yu, B. (2003). An assessment of uncalibrated CLIGEN in Australia. *Agricultural and Forest Meteorology*, 119, 131–148. [https://doi.org/10.1016/S0168-1923\(03\)00141-2](https://doi.org/10.1016/S0168-1923(03)00141-2)
- Zhang, J. X., Chang, K.-T., & Wu, J. Q. (2008). Effects of DEM resolution and source on soil erosion modelling: A case study using the WEPP model. *International Journal of Geographical Information Science*, 22, 925–942. <https://doi.org/10.1080/13658810701776817>
- Zhang, X. C. (2005). Spatial downscaling of global climate model output for site-specific assessment of crop production and soil erosion. *Agricultural and Forest Meteorology*, 135, 215–229. <https://doi.org/10.1016/j.agrformet.2005.11.016>
- Zhang, X. C. (2016). Adjusting skewness and maximum 0.5 hour intensity in CLIGEN to improve extreme event and sub-daily intensity generation for assessing climate change impacts. *Transactions of the ASABE*, 56, 1703–1713. <https://doi.org/10.13031/trans.56.10004>
- Zhang, X.-C., Chen, J., Garbrecht, J. D., & Brissette, F. P. (2012). Evaluation of a weather generator-based method for statistically downscaling non-stationary climate scenarios for impact assessment at a point scale. *Transactions of the ASABE*, 55, 1–12. <https://doi.org/10.13031/2013.42366>
- Zhang, X. C., & Nearing, M. A. (2005). Impact of climate change on soil erosion, runoff and wheat productivity in central Oklahoma. *Catena*, 61, 185–195. <https://doi.org/10.1016/j.catena.2005.03.009>
- Zhang, X. C., Nearing, M. A., Garbrecht, J. D., & Steiner, J. L. (2004). Downscaling monthly forecasts to simulate impacts of climate change on soil erosion and wheat production. *Soil Science Society of America Journal*, 68, 1376–1385. <https://doi.org/10.2136/sssaj2004.1376>

How to cite this article: Mullan D, Matthews T, Vandaele K, et al. Climate impacts on soil erosion and muddy flooding at 1.5 versus 2°C warming. *Land Degrad Dev.* 2019;30:94–108. <https://doi.org/10.1002/ldr.3214>